Available online at www.sciencedirect.com

ScienceDirect

Trans. Nonferrous Met. Soc. China 20(2010) 201−206

Transactions of Nonferrous Metals Society of China

www.tnmsc.cn

Effect of Al content on high temperature erosion properties of arc-sprayed FeMnCrAl/Cr_3C_2 coatings

LUO Lai-ma(罗来马)[1], LIU Shao-guang(刘少光)[2], YU Jia(俞 佳)[1], LUO Juan(罗 娟)[1], LI Jian(郦 剑)[1]

1. Department of Materials Science and Engineering, Zhejiang University, Hangzhou 310027, China;
2. Wenzhou Cadre New Special Material Co. Ltd., Wenzhou 325029, China

Received 17 December 2008; accepted 7 April 2009

Abstract: Three types of FeMnCrAl/Cr_3C_2 coatings with different Al content were deposited on 20# steel substrates by the high velocity arc spraying (HVAS) process. Surface microstructures of the coatings were analyzed by optical microscopy (OM) and X-ray diffractometry (XRD). High temperature erosion (HTE) tests were performed in an erosion tester at different impact angles. The surface morphologies of the eroded coatings were observed on a field emission scanning electron microscope(FE-SEM). The laminated structure is found on all the prepared coatings with the porosity and oxide fraction in the coatings decreasing with the Al content from 0 to 15% (mass fraction). Sample FA3 with 15% Al, possessing the lowest porosity and oxide fraction, has the best HTE resistance, which demonstrates that Al addition can improve the HTE resistance of the coatings. The erosion rate of sample FA1 exhibits a maximum value at 90˚ impact angle. The maximum erosion rates of both FA2 and FA3 samples appear in the range of 60˚−90˚ impact angles. Erosion loss of the coatings occurs through brittle breaking, cutting and fatigue spalling.

Key words: high velocity arc spraying (HVAS); coating; erosion mechanism; high temperature erosion(HTE)

1 Introduction

Because of high fractions of ash and sulphide of the coals for power station, high temperature erosion (HTE) is one of the main failure modes of the circulating fluidized bed boiler[1−3]. Many researches and approaches have been reported for reducing the erosion damage, one of which is thermal spraying coating, for example, Cr_3C_2-NiCr, WC-Co-Cr cermet coatings by high velocity oxygen-fuel (HVOF) spraying, Ni-based cermet coatings by plasma spraying, FeNiCrB, 3Cr13, NiCr and NiCr-WC coatings by arc spraying[3−8]. Among various thermal spray techniques, arc spraying has been more widely employed because of its economic advantage and flexibility of operation. The researches on influencing factors of HTE resistance of thermal spraying coatings have been reported. BERGET et al[9] reported that the erosion resistance of the WC-Co-Cr coatings by HVOF spraying increased at low impact angle when increasing Cr content from 5% to 8.5% (mass fraction). Grain size distribution of powder was found to be an important influencing factor of HTE resistance. Powder with narrow grain size distributions gave coatings better HTE resistance than that with wider grain size distributions[9]. JI et al[3] reported that the small carbide particles in the Cr_3C_2-NiC coatings by HVOF spraying can lead to a reduction of lamellae thickness and consequently an improved erosion performance[3]. The previous study[10] showed that the high temperature erosion resistance of the arc-sprayed coatings fabricated with the protection of nitrogen was significantly improved compared with the unprotected one. Little reports have been presented about the effect of Al content on microstructure and HTE resistance of arc-sprayed coatings.

More than 85% spray coating materials are alloys, and nickel-based alloys take half the spray material market share in China[11]. Because nickel is the expensive element and strategic resource, scientists and technicians have ever researched to substitute or reduce the consumption of nickel element. Manganese- based alloys are considered substitute materials for nickel-based alloy in some industrial fields because of their good corrosion resistances, wear resistances and low costs[12]. The previous study showed that arc-sprayed FeMnCr/Cr_3C_2 coating on low carbon steel possessed good erosion resistance compared with the

Foundation item: Project(2009C31129) supported by the Science and Technology Department of Zhejiang Province, China
Corresponding author: LI Jian; Tel/Fax: +86-571-87952853; E-mail: metal@zju.edu.cn
DOI: 10.1016/S1003-6326(09)60121-7

same steel, but arc-sprayed $FeMnCr/Cr_3C_2$ coating had higher porosity and oxide fraction than arc-sprayed $FeNiCr/Cr_3C_2$ coating.

In this work, the influence of Al content on microstructure and HTE resistance of $FeMnCr/Cr_3C_2$ coatings was studied. Three types of samples with Al contents of 0, 8% and 15% (mass fraction) were applied. The samples were prepared on $20^{\#}$ steel (0.17%−0.24% C, mass fraction) substrates by high velocity arc spraying(HVAS) process with the cored wire. The HTE resistance of coatings was evaluated in an elevated temperature erosion tester, simulating the service conditions of the boiler. The microstructures of arc-sprayed coatings were analyzed by optical microscopy(OM) and X-ray diffractometry(XRD). The surface morphologies of the eroded coatings were analyzed by field emission scanning electron microscopy (FE-SEM). And the erosion mechanism was discussed.

2 Experimental

2.1 Deposition of coating

Commercially available Mn, FeSi, Al, Fe, Cr_3C_2 and Cr powders were employed as core materials in this study. The powders were dried and sieved through the micron standard sieve for cored wires fabrication. The compositions of three types of core materials are shown in Table 1. $FeMnCr/Cr_3C_2$, $FeMnCr8Al/Cr_3C_2$, $FeMnCr15Al/Cr_3C_2$ coatings are referred to FA1, FA2 and FA3, respectively.

Table 1 Compositions of core materials (mass fraction, %)

Sample	Mn	Cr	Al	FeSi	Cr_3C_2	Fe
FA1	50	14	0	2	20	Bal.
FA2	50	14	8	2	20	Bal.
FA3	49	14	15	2	20	Bal.

The cored wires were prepared using mild steel (0.08% C, mass fraction) strip with a cross-section of 12 mm×0.3 mm to wrap Ni, Cr, Al, Cr_3C_2 and Fe-Si powders. The strip was rolled to give a U-shaped cross-section by three pairs of rollers and then the powders were put in. The U-shaped strip was drawn to form cored wires with 2.5 mm in diameter. The filling volume ratio of the powder in the cored wires was 45%−50%.

$20^{\#}$ steel with dimensions of 70 mm×35 mm×4 mm was used as sample substrate. The surface was sand-blasted to give a surface finish of grade Sa3 and subjected to arc spraying immediately, using a CAS−400 arc spraying machine under air pressure of 0.8 MPa, voltage of 38 V and current of 260 A. The coating thickness was controlled to be 0.8 mm. The sample surface was treated for HTE tests. The microstructure analysis was performed according to metallographic sample preparation method.

2.2 Erosion test

The HTE test was carried out using an erosion tester, simulating processing condition for water pipe wall of the CFB boiler[1], as schematically illustrated in Fig.1. The test conditions are listed in Table 2. The erosion testing was carried out at 30°, 45°, 60° and 90° impact angles. The abrasive was angular Al_2O_3 particles with an average grain size of 170 μm. The morphology and the composition of the abrasives are shown in Fig.2.

The erosive rates were taken as the volume loss of samples per unit mass abrasive consumption. The mass loss after abrasives erosion was measured using a precise

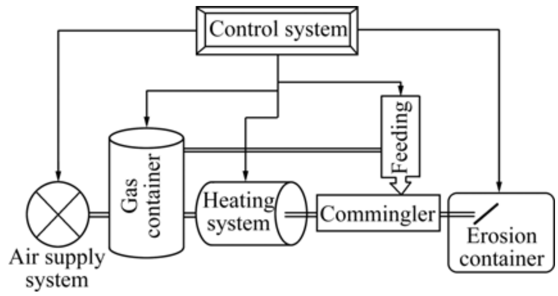

Fig.1 Schematic diagram of HTE tester

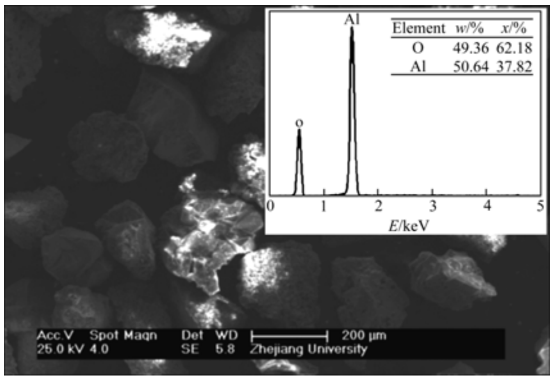

Fig.2 SEM morphology of abrasive particles with EDS results

Table 2 HTE test conditions

Item	Condition or value
Carrier gas	Air
Gas pressure/MPa	0.5
Gas velocity/($m \cdot s^{-1}$)	40
Gas temperature/℃	900
Sample temperature/℃	400
Impact angle/(°)	30−90
Erosive testing time/s	10
Abrasive mass/g	300
Abrasive size/μm	150−180
Abrasive	Multi-angular alumina

balance, with a weighing accuracy of 0.1 mg, which was then transformed to the volume loss. The erosive surfaces were analyzed by FE-SEM (Sirion, USA). The microstructures of coatings were analyzed by OM and XRD, (Rigaku D/max-rA type) with Cu K_α radiation, operated at 40 kV and 20 mA. Vickers hardness of the coatings was tested under a load of 0.98 N. The porosity and oxide fraction of coatings were measured using image analyzer.

3 Results and discussion

3.1 Coating characterization

The surface and the cross-section morphologies of the coatings are shown in Fig.3 and Fig.4, respectively. The physical characteristics of the coatings are listed in Table 3. It can be seen that FA1 coating without Al possesses higher porosity (black areas in Fig.3) and more oxide phases (grey areas in Fig.3) than coatings

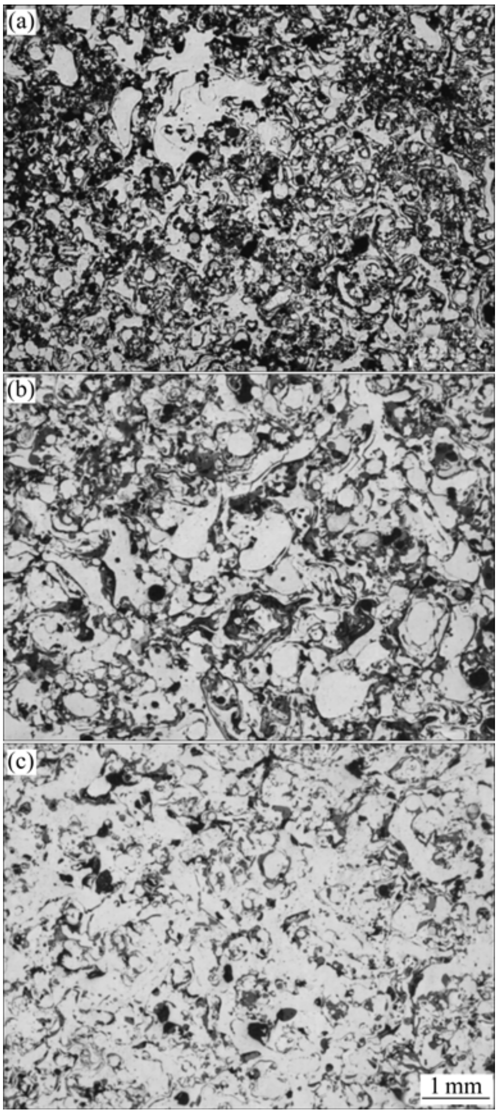

Fig.3 Surface morphologies of coatings: (a) FA1; (b) FA2; (c) FA3

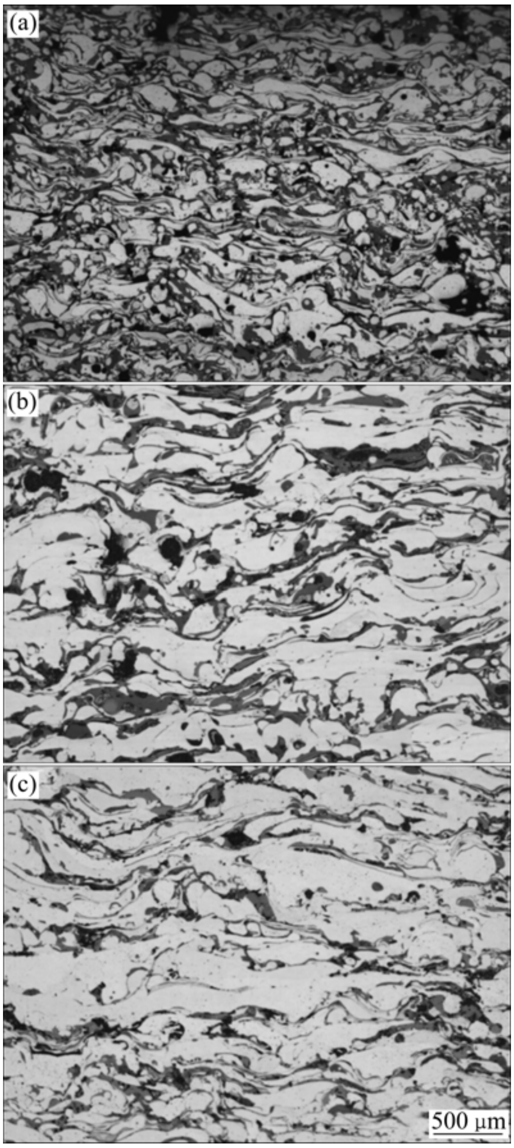

Fig.4 Cross-section morphologies of coatings: (a) FA1; (b) FA2; (c) FA3

Table 3 Hardness, porosity and oxide fraction of coatings

Coating	Hardness/GPa	Porosity/%	φ(Oxide)/%
FA1	4.27	6.2−8.7	20−24
FA2	4.11	4.1−5.8	14−15
FA3	3.96	< 3	8−10

containing Al element. Among the three types of coatings, FA3 coating shows a relatively heterogeneous microstructure with the lowest oxide fraction and porosity. It is shown in Fig.4 that the microstructure consists of lamellar splats interspersed with oxides and pores in all coatings, consistent with former studies [1, 13].

The EDS results of the oxides area interspersed into the lamellar splats of the three kinds of coatings are shown in Table 4. It can be found that Al and Cr elements of the oxides increase with the increasing Al content. Generally, it is considered that oxidizing during the spraying occurs through two main ways: 1) during the particle in-flight period; and 2) in the period shortly after the droplet impacts on substrate[13−14]. The coatings were prepared under the same processing condition, so the oxide fractions depend on the element compositions of the coatings. The heat of formation of Al_2O_3 is much larger than that of Fe or Mn oxide, and Al reacts with O more easily to form Al_2O_3. The preferential formation of Al_2O_3 inhibits the formation of other oxide phases during spraying. Therefore, with increasing Al content, oxide fraction and porosity decrease in the coatings[15−16].

Table 4 EDS results of oxides interspersed into lamellar splats of coatings (molar fraction, %)

Sample	O	Cr	Mn	Fe	Al
FA1	31.45	4.67	20.94	42.94	−
FA2	30.73	8.80	3.35	46.78	10.34
FA3	51.11	13.55	4.09	14.33	16.92

Fig.5 shows the XRD spectra of the coatings with the peaks of γ-Fe, α-Fe and iron oxide, respectively. The highest peak intensities of γ-Fe and iron oxide phases are observed for FA1 (without Al element). On the contrary, the lowest peak intensities of γ-Fe and iron oxide phases appear on the spectrum of FA3 coating. The result shows that Al element in the coatings effectively inhibits the formation of iron oxide phases. The XRD analysis is consistent with the results of Fig.3, Fig.4, Table 3 and Table 4.

3.2 Effect of impact angle

For ductile materials, the erosion damage usually attributes to fatigue spalling, cutting and ploughing of the surface, with the maximum damage taking place at lower impact angle. For brittle materials, the fatigue cracking and brittle breaking are the main reasons of the surface materials loss, with the maximum erosion appearing at higher impact angle[1]. Fig.6 shows the effect of impact angle on the erosion rate of the coatings and $20^{\#}$ steel. For $20^{\#}$ steel, the HTE resistance decreases with increasing the impact angle and the maximum erosion takes place at 30°, with typical ductile erosion behavior. It is remarkably found that at all impact angles, the erosion rate of all coatings is much lower than that of $20^{\#}$ steel and among the coatings FA1 exhibits the largest erosion rate. Under the 90° impact angle, the erosion rate reaches a maximum value for FA1 coating. This is because there are much more brittle oxide phases and high porosity on splat boundaries in FA1 coating, leading to relatively weak bonding and aggravating the lamellar

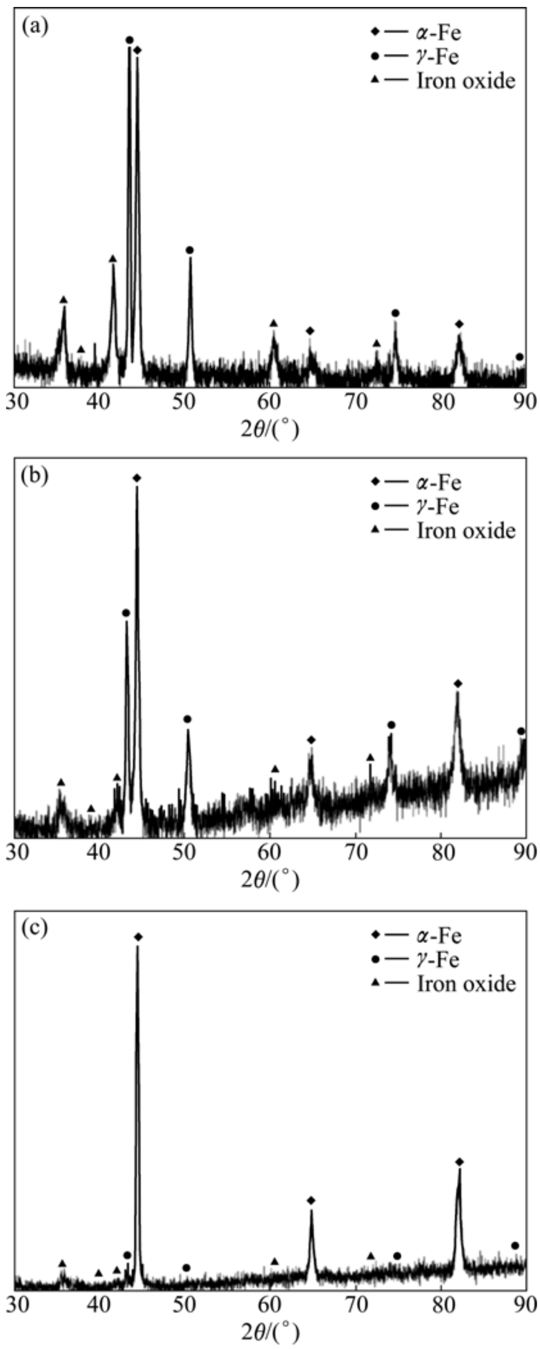

Fig.5 XRD patterns of coatings: (a) FA1; (b) FA2; (c) FA3

spalling and brittle breaking. The maximum erosion rate of FA2 coating appears in the impact angle of 90°. The impact angle changing from 45° to 90° has little effect on the erosion rate of FA2 coating. Sample FA3 shows the best THE resistance and a maximum erosion rate at 60° impact angle. As shown in Fig.3 and Table 3, FA3 coating containing 15% A1 has the lowest porosity and oxide fraction than FA1 and FA2 coatings. Therefore, the best erosion resistance of FA3 coating could be attributed to the finer microstructure and lower porosity and oxide fraction.

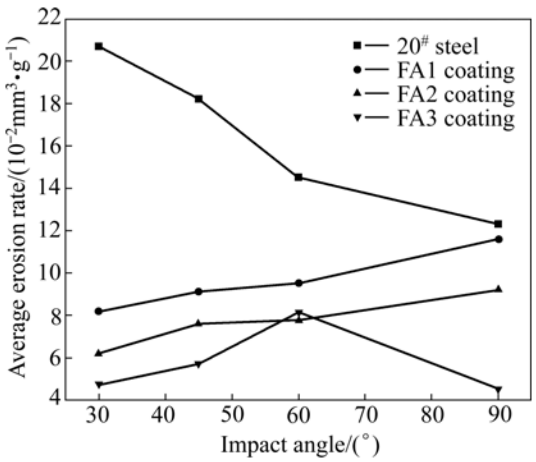

Fig.6 Effect of impact angle on erosion rate

3.3 Morphology of eroded surfaces

Fig.7 shows the surface morphologies of FA1 and FA3 coatings eroded at 60° impact angle. The brittle breaking, fatigue spalling and cutting can be observed for FA1 coating on worn surface (Fig.7(a)). The high magnification image (Fig.7(b)) of cutting areas (arrow 1 in Fig.7(a)) shows that the large size brittle breaking and cracking can be clearly seen. Fig.7(c) shows the morphology of the FA3 worn surface at 60° impact angle. The cutting and fatigue spalling can be observed as well, but without large size fracture. In high magnification (Fig.7(d), the area (arrow 2 in Fig.7(c)) manifests brittle micro-breaking and chipping by abrasives. The result shows that the lower porosity and oxide fraction of coatings can hinder serious surface material removal.

When brittle oxides are included in the splats boundaries, the impact of abrasives can easily damage the splat layer due to the brittle oxides weakening the bonding of splats. The loose microstructure and the existence of pre-cracks of the oxides increase the stress concentration under impacting, and cannot support surface materials effectively under impacting of the abrasive. Therefore, it is evident that brittle breaking and cracks easily initiate from the interface between oxides and splats and propagate along the lamellar interfaces under particle impacting, leading to lamellar spalling and brittle breaking (Fig.7(b)). The exposed fresh surface is subjected to the next cycle of particle impacting and consequently failures by abrasive erosion. As shown in Table 3, Fig.3(a) and Fig.4(a), FA1 coating contains more oxides and pores, leading to large size brittle breaking and crack formation (Fig.7(b)). FA3 coating possesses lower oxide fraction and porosity. It is clear from Fig.7(d) that finer microstructures limit large size brittle breaking and the crack formation. Therefore, the HTE results in Fig.6 are well explained that the oxide phases and pores in the coatings degrade the bond strength of the phases and hence the HTE resistance, and Al element addition can improve the HTE resistance of the arc-sprayed coatings.

4 Conclusions

1) FeMnCrAl-Cr_3C_2 coatings increase the HTE resistance of 20# steel.

2) FA3 coating with 15% Al which possesses the

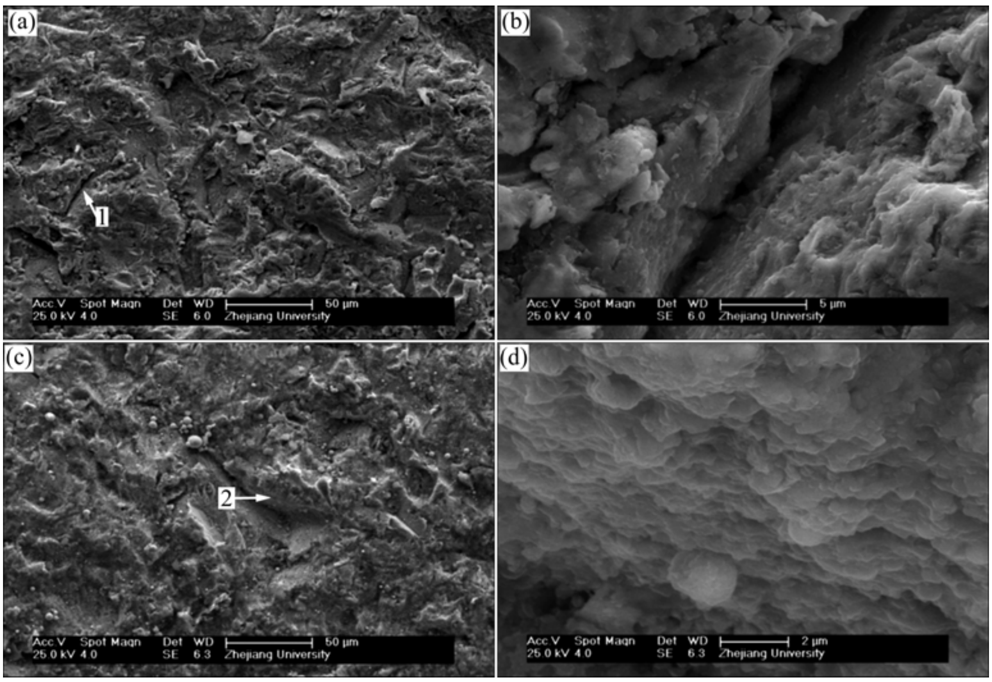

Fig.7 Morphologies of eroded surfaces for FA1 and FA3 coatings after erosion test at 60° impact angle: (a) FA1; (b) Zone 1 in Fig.7(a); (c) FA3; (d) Zone 2 in Fig.7(c)

lowest porosity and oxide fraction exhibits the best HTE resistance. The addition of Al can improve HTE resistance of the arc-sprayed coatings.

3) Erosion of the coatings occurs through brittle breaking, cutting and fatigue spalling. Material losses of FA1 and FA3 coatings are caused by large size brittle breaking cutting and brittle micro-breaking, respectively.

References

[1] LIU Shao-guang, WU Jin-ming, ZHANG Sheng-cai, RONG Shu-jie, LI Zhi-zhang. High temperature erosion properties of arc-sprayed coatings using various cored wires containing Ti-Al intermetallics [J]. Wear, 2007, 262: 555−561.

[2] VENUGOPAL, AGRAWAL M. Evaluation of arc sprayed coatings for erosion protection of tubes in atmospheric fluidised bed combustion (AFBC) boilers [J]. Wear, 2008, 264: 139−145.

[3] JI Gang-chang, LI Chang-jiu, WANG Yu-yue, LI Wen-ya. Erosion performance of HVOF-sprayed Cr_3C_2-NiCr coatings [J]. Journal of Thermal Spray Technology, 2007, 16: 557−565.

[4] STACK M M, PENA D. Particle size effects on the elevated temperature erosion behaviour of Ni-Cr/WC MMC-based coatings [J]. Surface and Coatings Technology, 1999, 113: 5−12.

[5] DU Ling-zhong, XU Bin-shi, DONG Shi-yun, YANG Hua, WU Yi-xiong. Wear behavior of high velocity arc sprayed 3Cr13 steel coating in oil containing sand [J]. Transactions of Nonferrous Metals Society of China, 2004, 14(s1): 370−373.

[6] CHEN Yong-xiong, XU Bin-shi, LIU Yan, LIANG Xiu-bing, XU Yi. Structure and sliding wear behavior of 321 stainless steel/Al composite coating deposited by high velocity arc spraying technique [J]. Transactions of Nonferrous Metals Society of China, 2008, 18: 603−605.

[7] LI Chang-jiu, YANG Guan-jun, OHMORI A. Relationship between particle erosion and lamellar microstructure for plasma-sprayed alumina coatings [J]. Wear, 2006, 260: 1166−1172.

[8] MISHRA S B, CHANDRA K, PRAKASH S. Characterisation and erosion behaviour of NiCrAlY coating produced by plasma spray method on two different Ni-based superalloys [J]. Materials Letters, 2008, 62: 1999−2002.

[9] BERGET J, ROGNE T, BARDAL E. Erosion-corrosion properties of different WC-Co-Cr coatings deposited by the HVOF process influence of metallic matrix composition and spray powder size distribution [J]. Surface and Coatings Technology, 2007, 201: 7619−7625.

[10] LIU Shao-guang, WU Jin-ming, ZHANG Sheng-cai, HU Xiao-hai, RONG Shu-jie, LI Zhi-zhang. Effect of nitrogen protective atmosphere on microstructure and property of nanocomposite coating [J]. Journal of Zhejiang University: Engineering Science, 2008, 42(3): 493−497. (in Chinese)

[11] FUKUMOTO M. The current status of thermal spraying in Asia [J]. Journal of Thermal Spray Technology, 2008, 17: 5−13.

[12] ZHANG Yan-sheng, SHI Chang-xu. Study of Fe-Mn-Al austenitic steel, heat-resistant steel, non-magnetic steel and low temperature steel [J]. Acta Matallurgica Sinica, 1964, 7: 285−299.

[13] NEWBERY A P, GRANT P S. Oxidation during electric arc spray forming of steel [J]. Journal of Materials Processing Technology, 2006, 178: 259−269.

[14] LI C J, LI W Y. Effect of sprayed powder particle size on the oxidation behavior of MCrAlY materials during high velocity oxygen-fuel deposition [J]. Surface and Coatings Technology, 2002, 162: 31−41.

[15] DOBLER K, KREYE H, SCHWETZKE R. Oxidation of stainless steel in the high velocity oxygen-fuel process [J]. Journal of Thermal Spray Technology, 2000, 9: 407−413.

[16] POKHMURSKA H, DOVHUNYK V, STUDENT M, BIELANSKA E, BELTOWSKA E. Tribological properties of arc sprayed coatings obtained from FeCrB and FeCr-based powder wires [J]. Surface and Coatings Technology, 2002, 151/152: 490−494.

(Edited by YANG Bing)